energies

MDPI

Article

Concept Research of a Countermeasure Device for Preventing Scour around the Monopile Foundations of Offshore Wind Turbines

Wenxian Yang * and Wenye Tian

School of Engineering, Newcastle University, Newcastle upon Tyne NE1 7RU, UK; tianwenye@hotmail.com
* Correspondence: wenxian.yang@ncl.ac.uk; Tel.: +44-191-208-6171

Received: 23 August 2018; Accepted: 26 September 2018; Published: 28 September 2018

Abstract: Scouring has long been considered to be a major issue affecting the reliability of the monopile foundations of offshore wind turbines (OWTs) on sandy seabeds. To reduce the impact of scouring, several tons of rock/stone are usually placed around the foundations shortly after the installation of them. Such a measure is costly. Moreover, rock and stone may spread widely on the seabed during the long-term service period of OWTs. It has no doubt that recycling these rock and stone on the seabed is quite difficult in future decommission. For this reason, a new scour-countermeasure device (SEMCD) is proposed and studied in this paper. Considering that the major driver of scouring is horseshoe vortices around the monopile foundation, a hollow horn-like SEMCD with an arc surface profile is designed for weakening the horseshoe vortices. The SEMCD is made of either cement or other kinds of corrosion resistant materials. It is light in weight, and easy to install and decommission. In the paper, the working mechanism of the SEMCD is first explained. Then, its scouring mitigation effect (SME), i.e., its contribution to the reduction of horseshoe vortices and the mitigation of seabed erosion around the foundation, is studied through investigating its influences on down/up-flow and seabed shear stress. Finally, the optimal size of the SEMCD is discussed through investigating the impact of its size on the speeds of up and down flows and the shear stress on seabed surface. The calculation results have shown that the proposed SEMCD has great potential to prevent scouring and seabed erosion, so that it is of significance to improve the reliability of the monopile foundations of OWTs.

Keywords: scour; offshore wind turbine; monopile foundation; scouring mitigating device

1. Introduction

Despite the economic recession, the wind industry continues to grow worldwide. Particularly, the offshore wind industry is rapidly growing in recent years [1]. Moreover, its growing tendency will continue in the following years, attributing to abundant wind power resources at offshore sites. In addition, as visual impact and noise issues are absent from offshore wind farms, offshore wind turbines (OWTs) can be much larger in size as opposed to their onshore counterparts. At present, the capacity of main-stream OWTs is about 3 MW. However, larger OWTs, such as the 10 MW SeaTitan, 10 MW Sway Turbine ST10, 8 MW Areva, 8 MW Vestas V-164, and 7 MW Samsung S7.0-171, are on the way to the market [2]. The successful development of these large MW-scale turbines will certainly reduce the average cost of offshore wind projects, and therefore make offshore wind power more affordable for human use.

Despite the promising future, the exploration of offshore wind power is never easy. It is challenged by many issues, one of which is the lack of proven foundation technology. So far, various concepts of OWT foundations have been developed, such as monopile, gravity based structure, jacket, tripod,

suction bucket, and so forth. However, as monopile foundation technology is relatively more mature than other contenders, currently over 87% of existing OWTs use monopiles for support [1,3]. However, early practice has shown that the reliability of monopile foundations, particularly those placed on sand and soft clay seabed, are significantly affected by scouring. This issue was first discovered at the Egmond aan Zee wind farm in the Netherlands. Dong Energy said that their windfarms at Burbo Bank and Gunfleet Sands were also affected by this fault, which caused turbines to be unreliable and even sink. Experts from Renewables UK, who represent wind farm developers, said it could cost £50 m to fix Britain's 336 turbines that are thought to be at risk [4].

Scouring is a phenomenon that is observed when tidal current passes the monopile. It will stir sand particles, pick them up, and transport them away from the monopiles. In the long-term, deep holes will form around the monopiles, which will threaten the stability of the foundations and even cause sinking of the turbines in the worst case. A similar issue can be also observed from bridge piers. In order to address this issue, much effort has been spent in the past decades [5–24], most of which is concerned with the protection of bridge piers, and only a few are for protecting OWT foundations. The achievements of these studies can be roughly classified into two groups; one is through bed-armoring, and another is by flow-altering. In the first group, hard engineering materials, such as block, rack riprap, gravel bags, matrasses, and tetra pods, are placed on the seabed surrounding the pier to prevent excessive scouring [5–7,9,10,13,14]; In the second group, additional devices, such as sacrificial piles [16], delta-wing-like fins, and submerged vanes in front of the piers [8], collars on the piers, and slots through the piers [12,15,17,18,21], and surface guide panels [22], are employed to alter the flow around the piles to avoid the direct scouring of seabed. A more detailed review of these countermeasures can be found from [19,20]. As opposed to the first group of measures that use expensive hard engineering materials, the second group of countermeasures that use flow-altering devices are more cost-effective. However, their application is sometimes challenged. For example, the slot may be blocked by floating debris and thus lose its effectiveness [20]; sacrificial piles can reduce scour depth under clear water conditions, but they are less effective under live-bed conditions due to the passage of bed forms. Therefore, sacrificial piles are usually not recommended unless the flow remains aligned and the flow intensity is relatively small [16]; the surface guide panels are impractical because the stability of large-sized panels in front of piers cannot be guaranteed during floods [19]. Recently, a thin collar plate around the pier above the seabed level was investigated in the laboratory [20]. It shows an effect on scour protection. However, such a collar only shields a limited range of the seabed around the pier from being directly impacted by down-flow. It is weak in suppressing the vortices around the piers, and therefore it has a limited contribution to the mitigation of seabed erosion issues. Therefore, an effective scour countermeasure is still expected today, which motivates the research of this paper.

In this paper, an innovative horn-like scour-countermeasure device (SEMCD) is numerically studied through conducting computational fluid dynamics (CFD) calculations in ANSYS CFX [25]. More details about this research are reported below. Herein, it is worth noting that the work reported in this paper is mainly focused on the concept design of a new anti-scour device, and the feasibility study of its effect on preventing scour. Further validation research on the proposed device will be conducted at the next step, and relevant achievements will be reported in a separate paper.

2. Concept Design of the SEMCD

Scour takes effect mainly via horseshoe vortices and the vortices behind the pile foundation [20], which stirs sand particles on the seabed, picks them up, and transport them away from the wind turbine monopile foundation. As a consequence, a hole will be formed around the monopile. That will decrease the stability of the monopile foundation, and even cause sinking of the turbine, in the worst case. In view of the present expensiveness of bed-armoring countermeasures and their difficulty of decommission, a new cost-effective SEMCD device is studied in the following. It is sketched in Figure 1.

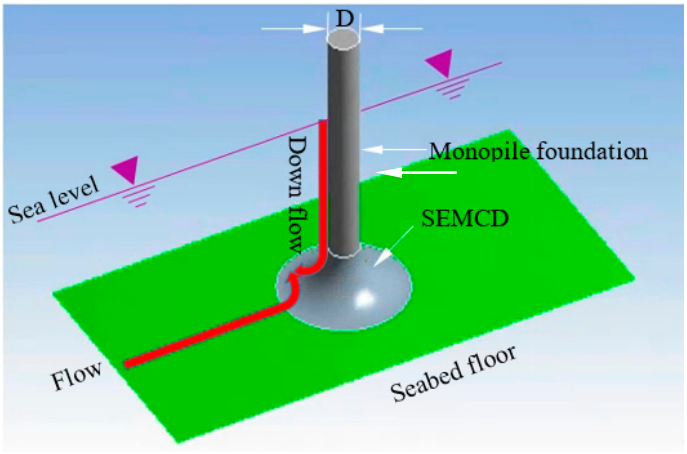

Figure 1. Schematic diagram of the proposed scour-countermeasure device (SEMCD).

As shown in Figure 1, the proposed SEMCD is installed directly on the seabed. It is a hollow structure, made of either cement or other kinds of corrosion-resistant materials. Therefore, it is light in weight, and easy to install, replace and recycle, as opposed to rock and stone. All of these merits make it more ideal to use at the site. Considering that the scouring process is driven mainly by the horseshoe vortices around the monopile foundation, the SEMCD takes the scouring mitigation effect (SME) by the combined use of the following two mechanisms, i.e.,

- Altering the streamlines of the current flow around the monopile foundation and guiding them to consume energy by each other (e.g., the energy of down-flow is consumed by up-flow, and vice versa), thus reduce the energy of horseshoes vortices;
- Breaking up the vortices via the specifically designed curve profiles of the SEMCD.

In ANSYS, the design of the surface profile of the SEMCD can be realized by following the steps below:

Firstly, one side of the monopile is selected (e.g., AB in Figure 2), and the intersection point between the monopile and seabed is found, i.e., point B in Figure 2;

Secondly, a line originating from point B is drawn, which is normal to the surface of the monopile (i.e., line BC in Figure 2);

Thirdly, an arc curve (i.e., $\hat{EF}$ in Figure 2) with radius R is drawn, which is tangential to both lines BC and AB;

Finally, the arc curve $\hat{EF}$ is rotated around the centerline (OO') of the monopile to form the horn-like surface profile of the SEMCD.

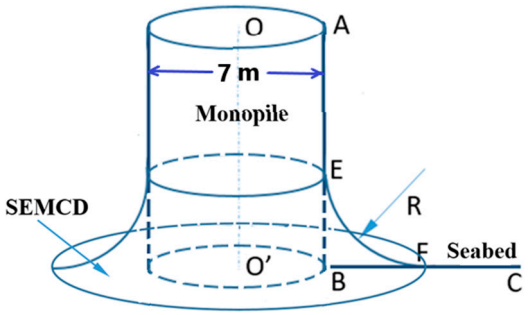

Figure 2. Design of the surface profile of the SEMCD.

Such a simple design method allows the size of the SEMCD to be easily changed by adjusting the radius R of the arc curve.

3. Site Description

In order to investigate the SME of the proposed SEMCD, the southern North Sea site (UK sector) is selected for calculations, where the water is about 31 m deep that is ideal for deploying monopole-supported OWTs. At this site, the depth-averaged spring tidal current speed is 0.53 m/s. The tidal ellipse is narrow with a semi-major axis of 0.53 m/s, and a semi-minor axis of 0.05 m/s. When the influences of ambient air temperature and water temperature were negligible, the standard empirical current profile, which has been found to fit well to a range of current observations [26], was used in the following research. It can be mathematically described as:

$$U(z) = \begin{cases} \left(\frac{z}{0.32h}\right)^{\frac{1}{7}} \overline{U} & (0 < z < 0.5h) \\ 1.07\overline{U} & (0.5h < z < h) \end{cases} \quad (1)$$

Then, the current speed profile shown in (1) is used to determine the input current based on the current speed of 0.7 m/s at a height of 0.32 h above the seabed [26]. The resultant oncoming current velocity profile is shown in Figure 3.

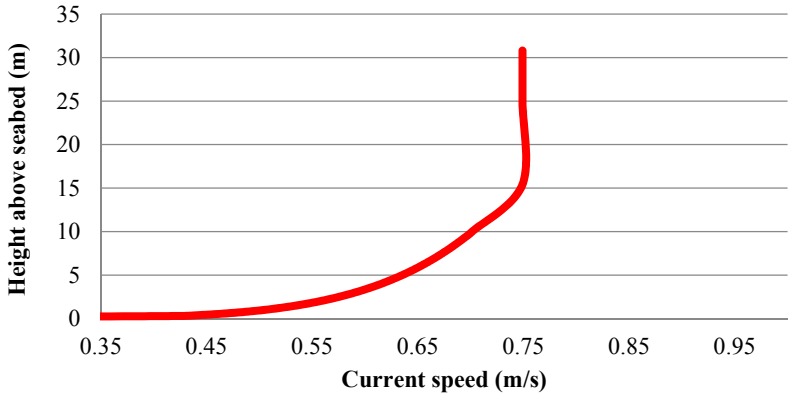

Figure 3. Flow velocity profile along the height above seabed.

4. Numerical Model for SME Analysis

Nowadays, a number of software has been developed to perform the numerical analysis of flow-solid interaction issues by the approach of CFD calculations. In this paper, ANSYS CFX [25] is adopted to investigate the SME of the proposed SEMCD. In the calculations, a monopile foundation with a diameter of 7 m was considered, which is used to support VESTAS' 8 MW OWT (i.e., V-164).

In the research, a fluid domain was defined first, which was 220 m long, 60 m wide, and 30.8 m high, see Figure 4. Such a fluid domain provides a large enough space for a wake region, thus allowing for a more accurate CFD calculation. The monopile foundation and the proposed SEMCD were placed in the middle of the domain, where different sizes of the SEMCDs can be applied.

In order to accurately simulate the scouring behavior while without causing excessive CFD calculations, a grid independence study was conducted first by trying different numbers of meshes to discretize the fluid domain. The resultant maximum shear stress on seabed surface was selected as a parameter for assessment. Its results obtained in different meshing cases are shown in Figure 5. In the process, different sizes of meshes were used to discretize the different regions in the fluid domain for ensuring calculation accuracy. For example, fine meshes were used to discretize the vicinity of the monopile foundation (i.e., the area within a distance of 40 m from the turbine foundation); coarse meshes were used to discretize the regions far from the monopile foundation (i.e., those beyond a distance of 40 m from the turbine foundation); and the central region of 24 m wide is discretized by using fine meshes. In the meantime, various cell types are used in combination, and different mesh densities are tested as well in the process of meshing. For example, proximity and curvature

types of cells were used in combination to discretize the curved surfaces of the monopile and SEMCD, so that the curved surfaces could be accurately modelled by much denser meshes. In the entire grid independence study, the maximum size of the cells that were far from the monopile was 4 m, while the minimum size of the cells near the monopile was only 0.5 m. They corresponded to the y^+ value ranges from 20 to 90.

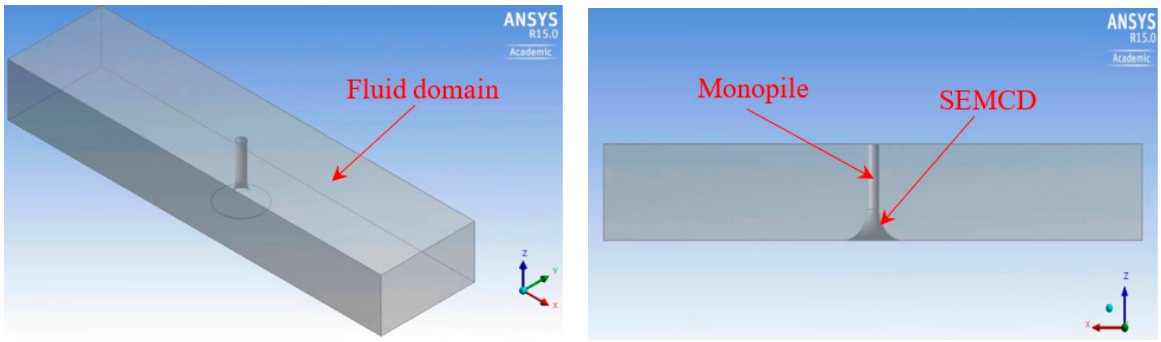

(**a**) (**b**)

Figure 4. Fluid domain and the numerical models of the SEMCD and the monopile foundation: (**a**) isometric view; (**b**) rear view.

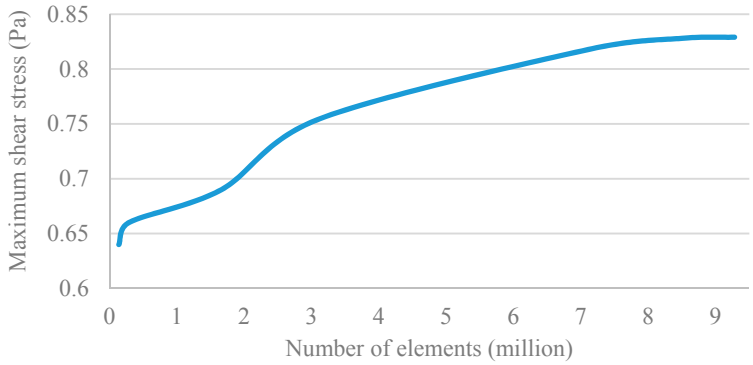

Figure 5. The influence of the numbers of mesh elements on the CFD calculation results.

From Figure 5, it is seen that the maximum shear stress on seabed surface reaches a stable value when the total number of mesh elements used for discretizing the fluid domain was 9.28 million. That implied that a reasonable accuracy of the calculation result has been achieved when the number of cells is as much as 9.28 million. Therefore, this number of mesh elements was adopted in the calculations in this paper for discretizing the fluid domain. The settings that are finally used for ANSYS CFX calculations are listed in Table 1.

Table 1. Settings in ANSYS CFX for meshing the domain of interest.

Parameter	Setting
Size function	Curvature
Initial size seed	Active assembly
Smoothing	Medium
Transition	Slow
Span angle center	Fine
Curvature normal angle	12.0°
Min size	0.01
Max face size	4.0 m
Max txt size	4.0 m
Growth rate	Default (1.20)
Use automatic inflation	Program controlled
Inflation option	First aspect ratio
Fir aspect ratio	5
Maximum layers	5
Triangle Surface Mesher	Program controlled
Topology checking	Yes
Pinch tolerance	Default (0.009 m)

An example of the resultant meshing results obtained when the number of mesh elements is 9.28 million, is shown in Figure 6. From Figure 6, it was seen that the meshes were indeed concentrated with higher density around the monopile foundation, whereas the meshes were less dense in the other regions of the domain.

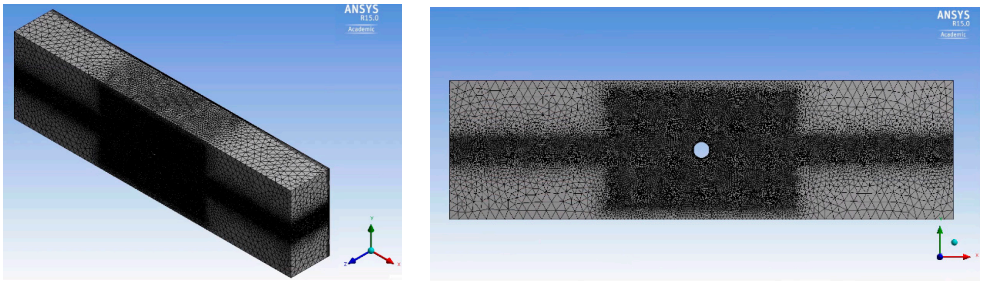

(**a**) (**b**)

Figure 6. An example of meshing results: (**a**) isometric view; (**b**) top view.

Subsequently, the fluid in the defined domain was assumed to be a single-phase fluid, and then the SST turbulence model was taken for implementing the simulation calculation, which accounted for the transport of the turbulent shear stress, and was anticipated to give an accurate prediction for the onset and the amount of flow separation under adverse pressure gradients [27–29]. The SST turbulence model simulations were performed with a Reynolds-average Navier–Stokes equation (RANS). Herein, it is worth noting that the SST with the RANS model was employed in this paper, attributing to its efficient and reasonable prediction to many flows, although it lacked the physical description of the turbulence-induced secondary flows and transitional flows between turbulent and laminar. For a stationary, viscous and incompressible Newtonian fluid, the RANS equation is [30]:

$$\rho \overline{U}_j \frac{\partial \overline{U}_i}{\partial x_j} = \rho \overline{f}_i + \frac{\partial}{\partial x_j}\left[-\overline{p}\delta_{ij} + \mu\left(\frac{\partial \overline{U}_i}{\partial x_j} + \frac{\partial U_j}{\partial x_i}\right) - \rho\overline{U_i' U_j'}\right] \quad (2)$$

where x_i ($i = 1, 2, 3$) are the Cartesian coordinates, U_i are the Cartesian components of the velocity, U_i' the fluctuating components of the velocity, f_i the components of the body forces, ρ the water density, p the pressure, δ_{ij} the Kronecker delta, μ the viscosity, and $\overline{[\cdot]}$ denotes the time-average operator. The left hand side of the equation represents the change in mean momentum of the fluid element,

owing to the unsteadiness in the mean flow and the convection by the mean flow. The first term in the right hand side of the equation is the mean body force, the term in the square brackets represents the sum of the three stresses. $\overline{p}\delta_{ij}$ is from the mean pressure field, $\mu\left(\frac{\partial \overline{U_i}}{\partial x_j}+\frac{\partial U_j}{\partial x_i}\right)$ from the viscous stress, and Reynolds stresses are $\rho\overline{U_i'U_j'}$ from the fluctuating velocity field.

The SST turbulence model is a two-equation eddy-viscosity model, which takes advantage of the superiorities of both the k-ε and the k-ω models. The former performs reasonably well for two-dimensional thin shear-flows in which the streamline curvature and the pressure gradient are small. For boundary layers with strong pressure gradients, and for flows with adverse pressure gradients, it performs poorly. It is also inaccurate for separated flows; the latter is more accurate than the former in modeling near-wall interactions. However, it can over-predict the shear stresses of adverse pressure gradient boundary layers. Additionally, it has issues with free stream flows, and it is very sensitive to inlet boundary conditions. The SST model accounts for cross-diffusion, which better marries the k-ε and k-ω models. Using a blended function based on the wall distance, one can include cross-diffusion when it is away from the wall, but not near it. In other words, using the wall distance as a switch, SST works like k-ε in the far field, and k-ω near the target geometry. This is why the SST model is adopted in the research of this paper. Herein, it is necessary to note that in the SST turbulence model, the turbulent viscosity μ_T is assumed to be isotropic (i.e., it is same in all directions), although in reality, the turbulent viscosity is not homogeneous (i.e., it varies in space). Based on this assumption, the turbulence kinetic energy $k=\frac{1}{2}\rho\overline{U_i'U_i'}$, the turbulence frequency ω, and the kinematic eddy viscosity ν_T can be calculated by using the following equations [27–29]:

$$\begin{cases} \frac{\partial(\rho k)}{\partial t}+\frac{\partial}{\partial x_j}(\rho U_j k)=P_k-\beta^*\rho k\omega+\frac{\partial}{\partial x_j}\left[(\mu+\sigma_k\mu_T)\frac{\partial k}{\partial x_j}\right] \\ \frac{\partial(\rho\omega)}{\partial t}+\frac{\partial}{\partial x_j}(\rho U_j\omega)=\alpha\rho S^2-\beta\rho\omega^2+\frac{\partial}{\partial x_i}\left[(\mu+\sigma_\omega\mu_T)\frac{\partial\omega}{\partial x_j}\right]+2(1-F_1)\rho\sigma_{\omega 2}\frac{1}{\omega}\frac{\partial k}{\partial x_i}\frac{\partial\omega}{\partial x_i} \\ \nu_T=\frac{a_1 k}{max(a_1\omega, SF_2)} \end{cases} \quad (3)$$

where the blending functions F_1 and F_2 are:

$$\begin{cases} F_1=tanh\left\{\left\{min\left[max\left(\frac{\sqrt{k}}{\beta^*\omega y},\frac{500\nu}{y^2\omega}\right),\frac{4\sigma_{\omega 2}k}{CD_{k\omega}y^2}\right]\right\}^4\right\} \\ F_2=tanh\left[\left[max\left(\frac{2\sqrt{k}}{\beta^*\omega y},\frac{500\nu}{y^2\omega}\right)\right]^2\right] \end{cases} \quad (4)$$

with:

$$CD_{k\omega}=max\left(2\rho\sigma_{\omega 2}\frac{1}{\omega}\frac{\partial k}{\partial x_i}\frac{\partial\omega}{\partial x_i},10^{-10}\right) \quad (5)$$

P_k is a production limit used in the turbulence equation to avoid the build-up of the turbulent kinetic energy in stagnation region. It can be mathematically expressed as [27–29]:

$$P_k=min\left[\mu_T\frac{\partial U_i}{\partial x_j}\left(\frac{\partial U_i}{\partial x_j}+\frac{\partial U_j}{\partial x_i}\right),10\beta^*\rho k\omega\right] \quad (6)$$

S is the invariant measure of the strain rate, y is the distance to the nearest wall, ν is the kinematic viscosity, and parameters $a_1=0.31$, $\alpha_1=\frac{5}{9}$, $\alpha_2=0.44$, $\beta_1=\frac{3}{40}$, $\beta_2=0.0828$, $\beta^*=0.09$, $\sigma_{k1}=0.85$, $\sigma_{k2}=1$, $\sigma_{\omega 1}=0.5$, and $\sigma_{\omega 2}=0.856$.

The boundary conditions on the seabed, monopile, and the SEMCD were defined as no-slip boundaries with smooth wall roughness. The water surface (i.e., the top of the computational domain) was defined as a free-slip boundary condition to simulate the less frictional effect of the free sea surface. At the inlet, the boundary condition was defined as the velocity boundary with the current speed profile described by (1). The other sides of the computational domain were set as open boundaries

with zero relative pressure, which allowed flow in and out the domain. All these boundary conditions can be mathematically expressed as:

$$\begin{cases} U_i = 0, i = 1,2,3 & \text{on the solid surface of seabed, monopile and SEMCD} \\ \frac{\partial U_1}{\partial n} = 0 & \text{on water surface} \\ U_1 = U(Z), U_2 = 0, U_3 = 0 & \text{at inlet} \\ p = 0 & \text{at other sides} \end{cases} \quad (7)$$

The default option of medium intensity (5%) was used throughout the paper. The simulation model with the aforementioned boundary conditions is shown in Figure 7.

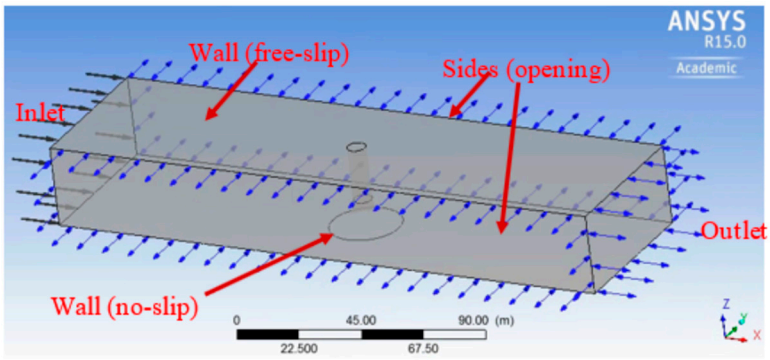

Figure 7. Simulation model with boundary conditions.

The software analysis settings for performing simulation calculations are listed in Table 2. In the calculations, the simulation iterated until the result converged and reached the predefined convergence criterion, where RMS was taken as the residual type, and the residual target was 10^{-5}. With the completion of the calculations, a number of flow characteristics, such as velocity vector, flow velocity, pressure, seabed shear stress and streamlines, are obtained. They will be used for further SME analyses.

Table 2. Software analysis settings for performing simulation calculations.

Parameter		Setting
Fluid model	Heat transfer	None
	Turbulence option	Shear stress transport
	Turbulence wall function	Automatic
Advection scheme option		High resolution
Turbulence numeric option		First order
Convergence control min. iterations		1
Convergence criteria max. iterations		500
Fluid timescale control		Auto timescale
Fluid length scale option		Conservative
Fluid timescale factor		1.0
Convergence criteria residual type		RMS
Convergence criteria residual target		10^{-5}

5. Simulation Results and Discussions

Various features are available in the ANSYS-CFX-CFD-Post as graphs, tables, contours, and streamlines, etc. Herein, three key features, i.e., velocity vector in the fluid domain, shear stress on seabed surface, and vertical velocity near seabed, are used for SME analysis. Among these features, velocity vector is used to indicate the flow direction, from which the potential scour can be inferred; shear stress on seabed surface and the vertical velocity near the seabed were used to assess the strength of scouring.

5.1. Operation Mechanism of the SEMCD

As mentioned above, scour emerges in the form of:

(1) down/up-flows in front of the monopile;
(2) horseshoe vortices at both sides of the monopile; and
(3) vortices in wake region behind the monopile.

Since all of these three types of behavior could be observed from the velocity vector, the calculated velocity vector was employed in the following to demonstrate the working mechanism of the SEMCD. For facilitating understanding, the operation mechanism of the SEMCD, and the flow behaviors in front and behind the monopile before and after using the SEMCD was investigated first. The calculation results of the velocity vector on the symmetric plane xz are shown in Figure 8. Figure 8a is the plane view, and Figure 8b shows the details of the flow in front of the monopile. The flow velocity is indicated by greyscale value, e.g., the red color indicates a larger value of velocity, and the dark blue color indicates a smaller value of velocity.

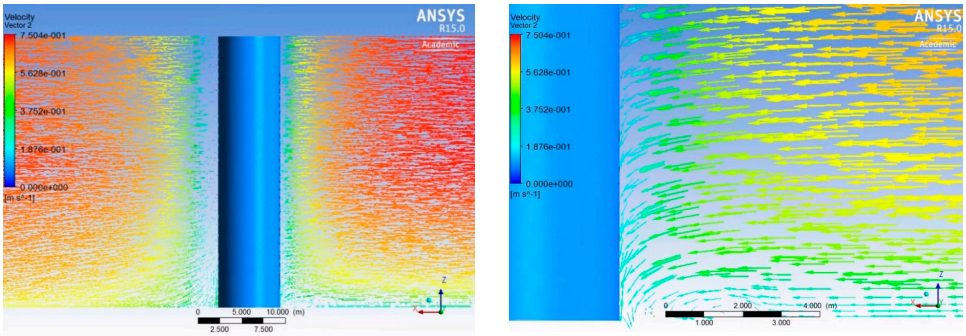

(**a**) (**b**)

Figure 8. Velocity vectors on the symmetric plane xz before using the SEMCD: (**a**) plane view; (**b**) details of the flow in front of the monopile.

From Figure 8b, it was clearly seen that the flow was diverted downward when it approached the monopile, i.e., the inline flow changed direction and form down-flow. Then, the down-flow stirred the seabed sediments (e.g., sand, soil, stones, etc.) and consequently led to seabed scouring.

Subsequently, a SEMCD with a geometric parameter of $R = 8$ m was installed on the monopile. Applying the same current velocity profile to the inlet of the fluid domain, the resultant velocity vectors on the symmetric plane xz are shown in Figure 9. Likewise, Figure 9a is the plane view, Figure 9b shows the details of the flow in front of the monopile.

From Figure 9b, it was found that after using the SEMCD, the down-flow observed in Figure 8b was significantly suppressed, and it could not be easily observed from the velocity vectors. Thus, it can be said that the proposed SEMCD did have potential to cancel the down-flow in front of the monopile.

Although Figures 8 and 9 have successfully demonstrated the contribution of the SEMCD to the cancellation of down-flow in front of the monopile, they are still unable to present a full description of the flow around the monopile in all circumferential directions. For this reason, the simulation results of the velocity vectors on a 0.1 m plane above the seabed are shown in Figure 10. Figure 10a shows the results obtained before using the SEMCD, and Figure 10b shows the results obtained after using the SEMCD.

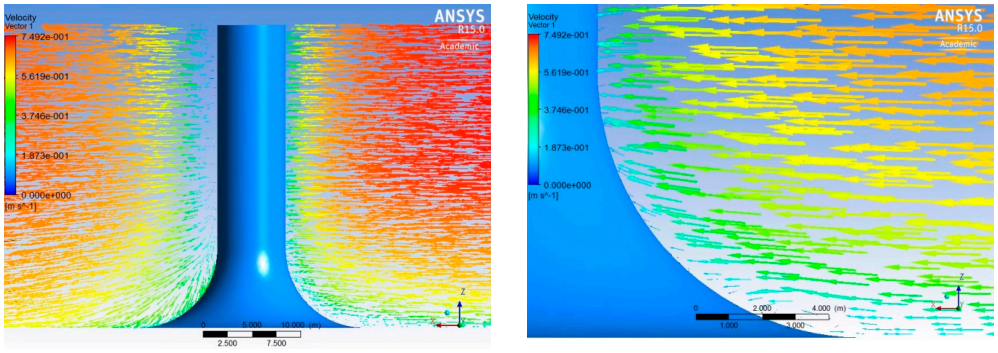

(**a**) (**b**)

Figure 9. Velocity vectors on the symmetric plane *xz* after using the SEMCD: (**a**) plane view; (**b**) details of the flow in front of the monopile

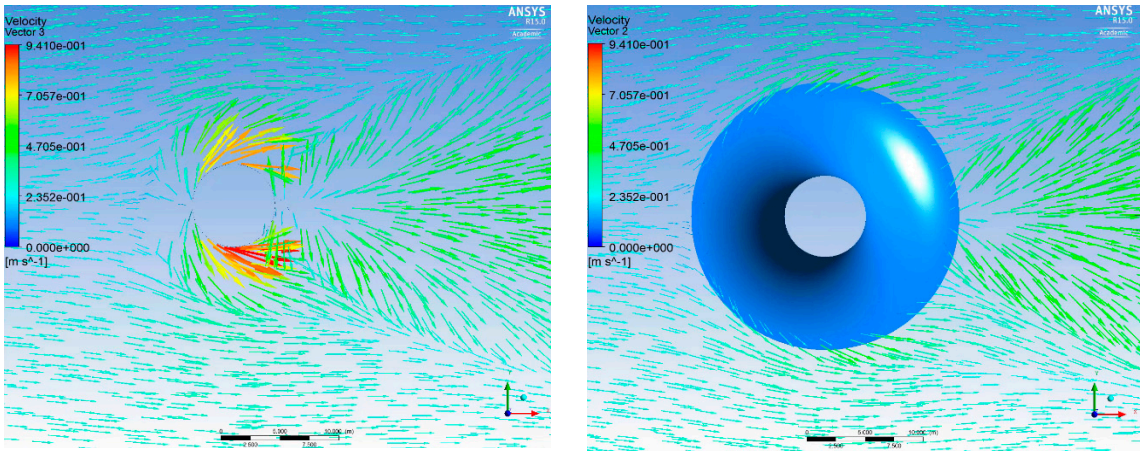

(**a**) (**b**)

Figure 10. Velocity vectors on the 0.1m plane above the seabed: (**a**) before using the SEMCD; (**b**) after using the SEMCD.

From Figure 10, it was found that on the plane of interest, the maximum flow velocity was reduced to be 0.51 m/s after using the SEMCD vs the maximum flow velocity of 0.95 m/s obtained before using the SEMCD. This means that the maximum flow velocity was reduced by about 50% by the SEMCD. This simulation results indicated that the proposed SEMCD does have potential to prevent scouring around monopile foundations as they reduced the velocity potential of the flow around the foundations.

Since it is known that seabed erosion will take place once the shear stress on seabed exceeds a certain value [26], shear stresses on seabed surface obtained under the same tidal current condition were investigated as well, in order to further investigate the SME of the SEMCD from the point of view of seabed erosion. The corresponding CFD calculation results are shown in Figure 11.

From Figure 11a, interestingly, it was found that there are four specific regions where seabed erosion is likely to happen as the shear stresses in these four regions are much larger than those in the other areas. Two of them are located at the two sides, while the other two are at the rear of the monopile. Moreover, the shear stresses at the two side areas are much larger in value, which indicates stronger scouring by horseshoe vortices. The comparison of Figure 11a,b shows that after using the SEMCD, the maximum shear stress was about 0.45 Pa, versus the maximum shear stress of 0.79 Pa obtained before using the SEMCD. This means that the application of the SEMCD results in over 40% of reduction in the maximum shear stress. Thus, the SEMCD is indeed helpful for preventing scouring and seabed erosion.

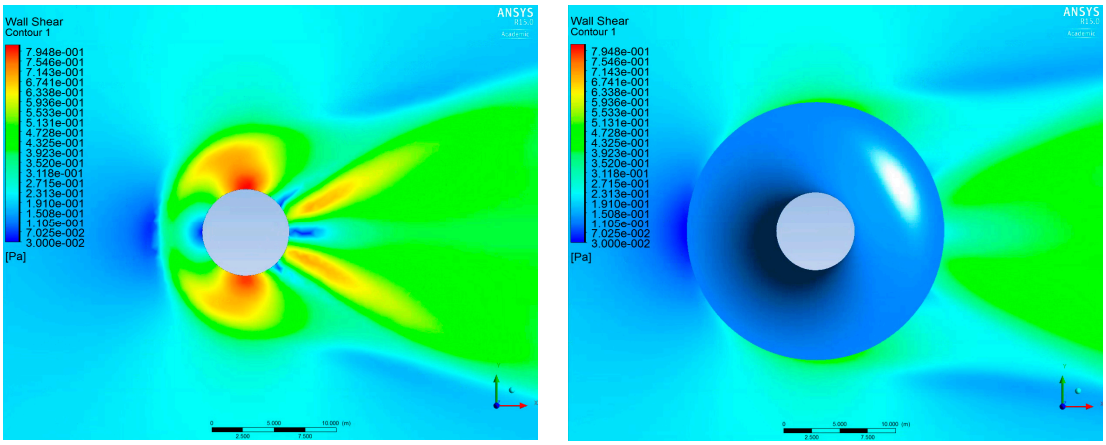

(**a**) (**b**)

Figure 11. Shear stress on the surface of seabed: (**a**) before using the SEMCD; (**b**) after using the SEMCD

Finally, considering that eddy viscosity can be used to characterize the transport and dissipation of vortex energy around the monopile, the eddy viscosities before and after using the SEMCD were calculated by using the Q-criterion method [31]. The corresponding calculation results are shown in Figure 12.

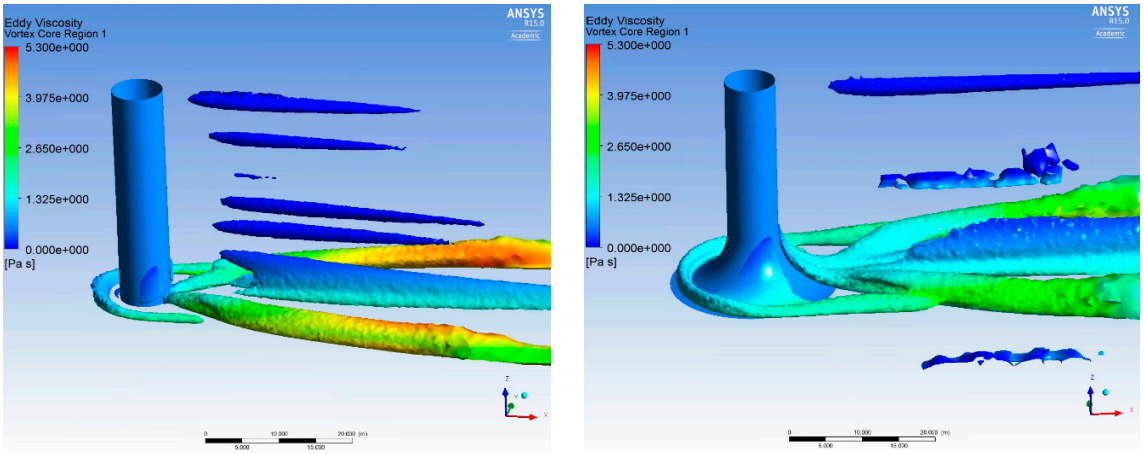

(**a**) (**b**)

Figure 12. Eddy viscosities: (**a**) before using the SEMCD; (**b**) after using the SEMCD.

From Figure 12, it is found that before using the SEMCD, stronger vortex energy is present behind the monopile. The maximum eddy viscosity value is about 5 Pa·s versus the maximum eddy viscosity value of about 3 Pa·s obtained after using the SEMCD. That means a 40% of reduction in the maximum eddy viscosity, attributing to the application of the SEMCD. Moreover, from Figure 12b, it was found that almost all horseshoe vortices were constrained on the surface of the SEMCD rather than directly on the seabed surface. It has no doubt that all of these merits of the SEMCD will benefit the prevention of scouring and seabed erosion.

5.2. Optimal Size of the SEMCD

As different sizes of SEMCDs may show different SME results, it is essential to optimize the size of the SEMCD so that the resultant SME can be maximized within the constraints of capital cost. For this reason, the variation tendencies of the maximum velocities of up- and down-flows on the plane 0.1 m above the seabed, and the maximum shear stress on seabed against increasing R are investigated in

this section. The maximum velocities of up- and down-flow were linked to the momentum of the flow stirring the seabed sediments around the monopile; while the maximum shear stress on seabed indicated the strength of scouring causing seabed erosion. The corresponding variation tendencies of the maximum velocities of up- and down-flow on the 0.1 m plane obtained when R increases from 0 m (i.e., absence of the SEMCD) to 10 m are shown in Figure 13.

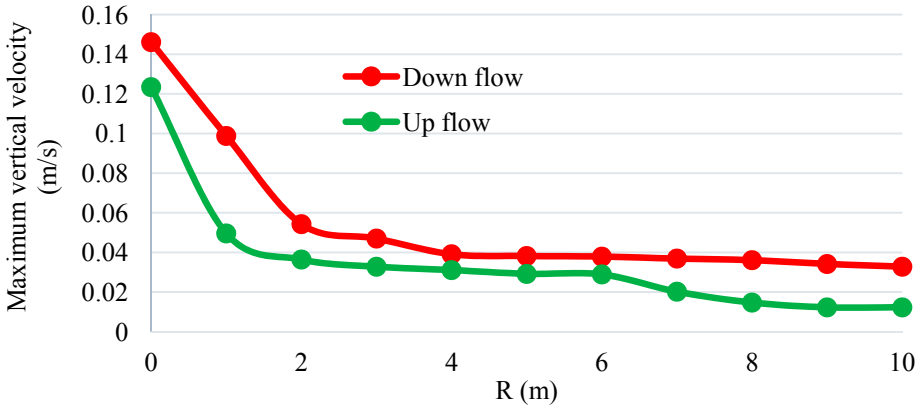

Figure 13. Variation tendencies of the maximum velocities of up- and down-flow.

From Figure 13, it was found that with the increase of the size of the SEMCD, the maximum velocities of both up-flow and down-flow showed monotonous decreasing tendencies. This implies that a larger SEMCD possesses a better capability of preventing scouring. However, in comparison, the SEMCD suppressed more of the up-flow than it does in suppressing the down-flow. This suggests that we could use the 'green curve' in Figure 13 to identify the optimal size of the SEMCD. Accordingly, the reduction rates of the maximum velocity of up-flow corresponding to different sizes of the SEMCDs are calculated and the corresponding results are listed in Table 3.

Table 3. Reduction rates of the maximum velocity of up-flow at different values of *R*.

R (m)	Maximum Velocity of Up Flow (m/s)	Reduction Rate (%)
0	0.1234	0.00
1	0.0496	59.80
2	0.0364	70.50
3	0.0328	73.41
4	0.0311	74.79
5	0.0292	76.33
6	0.0289	76.58
7	0.0202	83.63
8	0.0147	88.08
9	0.0123	90.03
10	0.0123	90.03

From Table 3, it is seen that the reduction rate showed a continuous decreasing tendency with the increase of *R* until the value of *R* reached 9 m. So, from the point of view of flow momentum, *R* = 9 m was regarded as the best size of the SEMCD for a monopile foundation with a diameter of 7 m.

In order to achieve a more reliable optimal size of the SEMCD, similar work was also carried out from the point of view of seabed erosion. The corresponding tendency of the maximum shear stress obtained when *R* increases from 0 m to 10 m is shown in Figure 14. The contours of the shear stress obtained when *R* = 4, 6, 8, and 10 m are also graphically illustrated for ease of understanding.

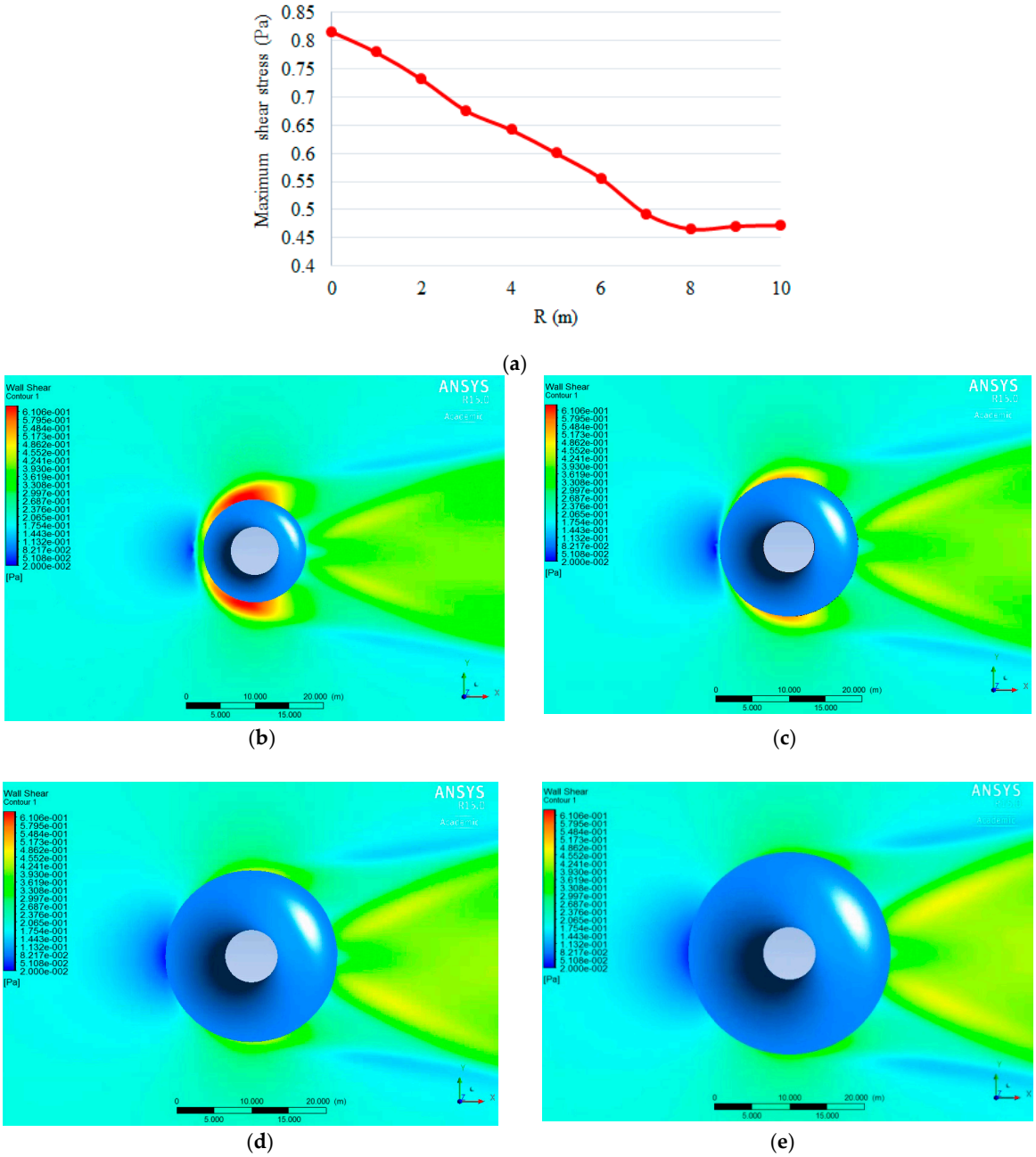

Figure 14. Variation of seabed shear stress vs. different sizes of the SEMCD: (**a**) Variation tendency of the maximum shear stress vs. the increasing R; (**b**) shear stress contour when R = 4 m; (**c**) shear stress contour when R = 6 m; (**d**) shear stress contour when R = 8 m; (**e**) shear stress contour when R = 10 m.

From Figure 14a, it is found that the maximum shear stress on the seabed also showed a monotonous decreasing tendency with increasing size of the SEMCD until the value of R reached 8 m, beyond which the maximum shear stress started to slightly increase, indicating enhanced seabed erosion and sediment transport. This slight increase can be also perceived from the comparison of Figure 14d,e. Based on this finding, from the point of view of seabed erosion, R = 8 m was the best size of the SEMCD for a monopile foundation with a diameter of 7 m. Such a finding is close to that obtained from Figure 13 and Table 3. In practice, the optimal size of the SEMCD could be compromised by financial cost.

6. Conclusions

Scouring has significant influence on the stability of OWT monopile foundations. In order to address this issue, a new concept of anti-scour device, namely the SEMCD, is studied in this paper. From the research reported above, the following conclusions are drawn:

- As opposed to the existing scour mitigation measures, the proposed SEMCD is easy to install, replace and decommission. Therefore, it is more ideal for site use;
- The SEMCD is effective in cancelling up- and down-flows, as well as horseshoes vortices around monopile foundations, which are the main drivers of the scouring process;
- After using the proposed SEMCD, the shear stress on seabed is reduced, which implies that the SEMCD does have the potential to prevent seabed erosion;
- The eddy viscosity results indicate that the maximum vortex energy is reduced by the SEMCD. Moreover, the horseshoes vortices are constrained on the surface of the SEMCD. All these merits will benefit the prevention of scour;
- A larger SEMCD can lead to better SME. For a 7 m diameter monopile foundation, $R = 8-9$ m is regarded as the best size of the SEMCD. However, in practice, the optimal size of the SEMCD will be compromised by its financial cost.

The numerical research reported above has demonstrated the potential of the proposed SEMCD in preventing scouring and seabed erosion around the foundations of OWTs. Subsequently, further validation studies will be conducted in laboratory, to verify its actual effect on reducing the chance of scour and seabed erosion. The relevant research will be reported in a separate paper.

Author Contributions: Conceptualization, W.Y.; Methodology and Validation, W.T.; Writing-Original Draft Preparation, W.Y.; Writing-Review & Editing, W.Y. and W.T.; Supervision, Project Administration and Funding Acquisition, W.Y.

Funding: This research was funded by the UK EPSRC, grant number EP/R021503/1.

Conflicts of Interest: The authors declare no conflict of interest.

Nomenclature

$U(z)$	Speed of tidal current at height z above the seabed
h	Water depth
$\overline{U}$	Depth-averaged current speed
(x, y, z)	Cartesian coordinates
U	Velocity
U'	Fluctuating velocity
f	Body force
ρ	Water density
p	Pressure
δ	Kronecker delta
μ	Viscosity
μ_T	Turbulent viscosity
ω	Turbulence frequency
ν_T	Kinematic eddy viscosity
k	Turbulence kinetic energy
P_k	Production
S	Invariant measure of strain rate
ν	Kinematic viscosity
F	Blending function
n	Normal direction
i, j	Indices for the scalar components of vectors

References

1. Offshore Wind in Europe. Key Trends and Statistics 2017. Available online: https://windeurope.org/wp-content/uploads/files/about-wind/statistics/WindEurope-Annual-Offshore-Statistics-2017.pdf (accessed on 27 September 2018).
2. Gupta, A. The World's 10 Biggest Wind Turbines. Available online: https://www.power-technology.com/features/featurethe-worlds-biggest-wind-turbines-4154395 (accessed on 29 September 2018).
3. The European Offshore Wind Industry–Key Trends and Statistics 2013. Available online: https://windeurope.org/wp-content/uploads/files/about-wind/statistics/European_offshore_statistics_2013.pdf (accessed on 27 September 2018).
4. Hundreds of Wind Turbines Could Be SINKING Due to Design Flaw. Available online: http://www.dailymail.co.uk/sciencetech/article-1265886/Sinking-turbines-cost-British-wind-farms-50million.html (accessed on 27 September 2018).
5. Posey, C.J. Test of scour protection for bridge piers. *J. Hydraul. Div.* **1974**, *100*, 1773–1783.
6. Brice, J.C.; Bloggett, J.C. *Countermeasures for Hydraulic Problems at Bridge Piers*; U.S Department of transportation: Washington, DC, USA, 1978.
7. Worman, A. Riprap Protection without Filter Layers. *J. Hydraul. Eng. ASCE* **1989**, *115*, 1615–1629. [CrossRef]
8. Gupta, A.K.; Gangadharaiah, T. Local scour reduction by a delta wing-lick passive device. In Proceedings of the 8th Congress of Asia and Pacific Regional Division, 2, CWPRS, Pune, India, 20–23 October 1992; pp. B471–B481.
9. Froehlich, D.C. Protecting bridge piers with loose rock riprap. *J. Appl. Water Eng. Res.* **2013**, *1*, 39–57. [CrossRef]
10. Chiew, Y.M. Mechanics of Riprap Failure at Bridge Piers. *J. Hydraul. Eng. ASCE* **1995**, *121*, 635–643. [CrossRef]
11. Hadfield, A.C. Sacrificial Piles as a Bridge Pier Scour Counter-Measure. Master's Thesis, University of Auckland, Auckland, New Zealand, 1997.
12. Chiew, Y.M. Scour protection at bridge piers. *J. Hydraul. Eng. ASCE* **1992**, *118*, 1260–1269. [CrossRef]
13. Chiew, Y.M.; Lim, F.H. Failure Behavior of Riprap Layer at Bridge Piers under Live-Bed Conditions. *J. Hydraul. Eng. ASCE* **2000**, *126*, 43–55. [CrossRef]
14. Lim, F.H.; Chiew, Y.M. Parametric Study of Riprap Failure around Bridge Piers. *J. Hydraul. Res.* **2001**, *30*, 61–72. [CrossRef]
15. Kumar, V.; Ranga Raju, K.G.; Vittal, N. Reduction of Local Scour around Bridge Piers Using Slot and Collar. *J. Hydraul. Eng. ASCE* **1999**, *125*, 1302–1305. [CrossRef]
16. Melville, B.W.; Hadfield, A.C. Use of sacrificial piles as pier scour countermeasures. *J. Hydraul. Eng. ASCE* **1999**, *125*, 1221–1224. [CrossRef]
17. Zarrati, A.M.; Gholami, H.; Mashahir, M.B. Application of collar to control scouring around rectangular bridge piers. *J. Hydraul. Res. IAHR* **2004**, *42*, 97–103. [CrossRef]
18. Zarrati, A.M.; Nazariah, M.; Mashahir, M.B. Reduction of local scour in the vicinity of bridge pier group using collars and riprap. *J. Hydraul. Eng. ASCE* **2006**, *132*, 154–162. [CrossRef]
19. Tafarojnoruz, A.; Gaudio, R.; Dey, S. Flow-altering countermeasures against scour at bridge piers: A review. *J. Hydraul. Res.* **2010**, *48*, 441–452. [CrossRef]
20. Mubeen, B.; Salman, B. Scour reduction around bridge piers: A review. *Int. J. Eng. Invent.* **2013**, *2*, 7–15.
21. Shatirah, A.; Noor, L.; Hossein, B.; Afshin, J. Reducing local scouring at bridge piles using collars and geobags. *Sci. World J.* **2014**. [CrossRef]
22. Huang, C.K.; Tang, C.J.; Kuo, T.Y. Use of surface guide panels as pier scour countermeasure. *Int. J. Sediment Res.* **2005**, *20*, 119–130.
23. Cho, Y.J.; Yang, K.S.; Kim, B.K. Development of counter measures against scouring at the toe of offshore wind turbine foundation. In Proceedings of the EWEA OFFSHORE 2015, Copenhagen, Denmark, 10–12 March 2015.
24. Stroescu, I.E.; Frigaard, P.; Fejerskov, M.; Nielsen, S.A. Scour design for self-protecting mono bucket foundation used for offshore wind turbines. In Proceedings of the EWEA OFFSHORE 2015, Copenhagen, Denmark, 10–12 March 2015.
25. AnsysCFX-Solver Theory Guide. Available online: https://www.scribd.com/document/146465149/ANSYS-CFX-Solver-Theory-Guide (accessed on 27 September 2018).

26. Soulsby, R.L. *Dynamics of Marine Sands*; Thomas Telford: London, UK, 1997.
27. Menter, F.R. Zonal Two Equation k-ω Turbulence Models for Aerodynamic Flows. In Proceedings of the 23rd Fluid Dynamics, Plasmadynamics, and Lasers Conference, Orlando, FL, USA, 6–9 July 1993.
28. Menter, F.R. Two-Equation Eddy-Viscosity Turbulence Models for Engineering Applications. *AIAA J.* **1994**, *32*, 1598–1605. [CrossRef]
29. SST k-Omega Model. Available online: http://www.cfd-online.com/Wiki/SST_k-omega_model (accessed on 2 September 2018).
30. Reynolds-Averaged Navier–Stokes Equations. Available online: https://en.wikipedia.org/wiki/Reynolds-averaged_Navier%E2%80%93Stokes_equations (accessed on 2 September 2018).
31. Hunt, J.C.R.; Wray, A.A.; Moin, P. *Eddies, Stream and Convergence Zones in Turbulent Flows*; Report CTR-S88; Centre for Turbulence Research: Moffett Field, CA, USA, 1988.